Auxiliary Material

1. Mg/Ca-SST Quality Control using Al/Ca, Mn/Ca and Weight per Foraminifera

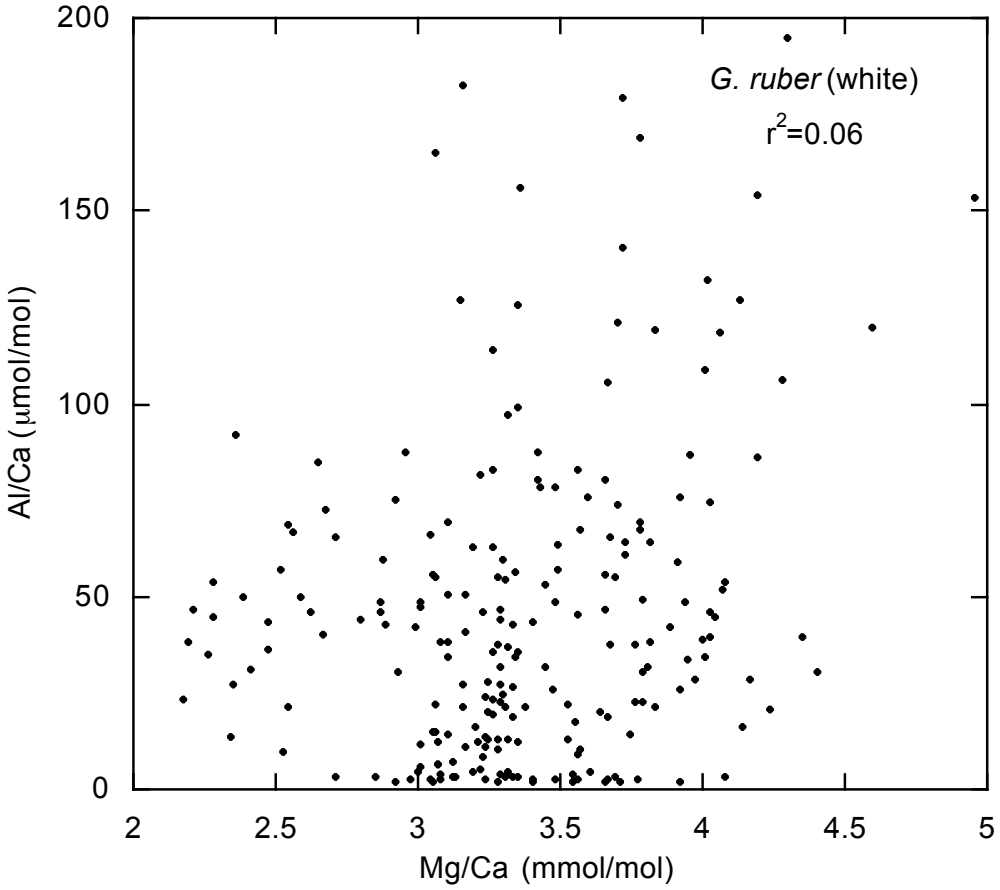

Figure S1. Comparison of culled *G. ruber* (white) Mg/Ca and Al/Ca data. The lack of correlation between Mg and Al suggests that Mg/Ca values are not influenced by insufficient clay removal. All Al concentrations below the limit of quantification (39 ppt) were set the 39 ppt.

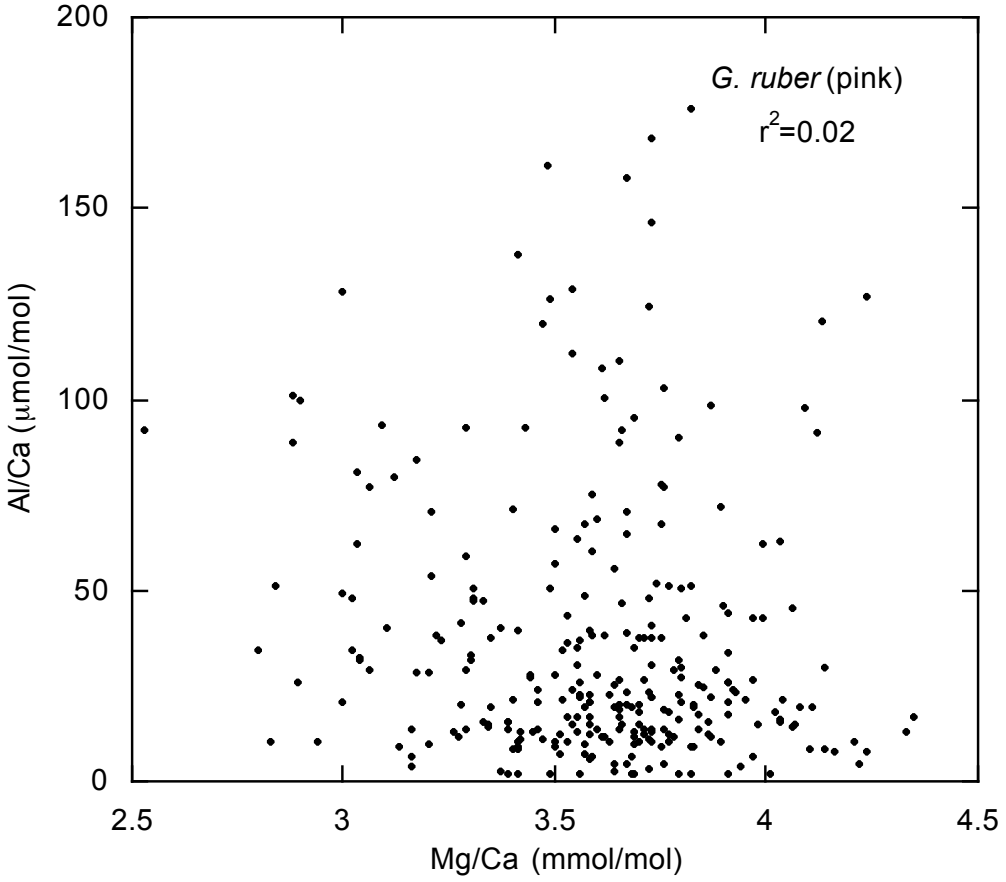

Figure S2. Comparison of culled *G. ruber* (pink) Mg/Ca and Al/Ca data. The lack of correlation between Mg and Al suggests that Mg/Ca values are not influenced by insufficient clay removal. All Al concentrations below the limit of quantification (39 ppt) were set the 39 ppt.

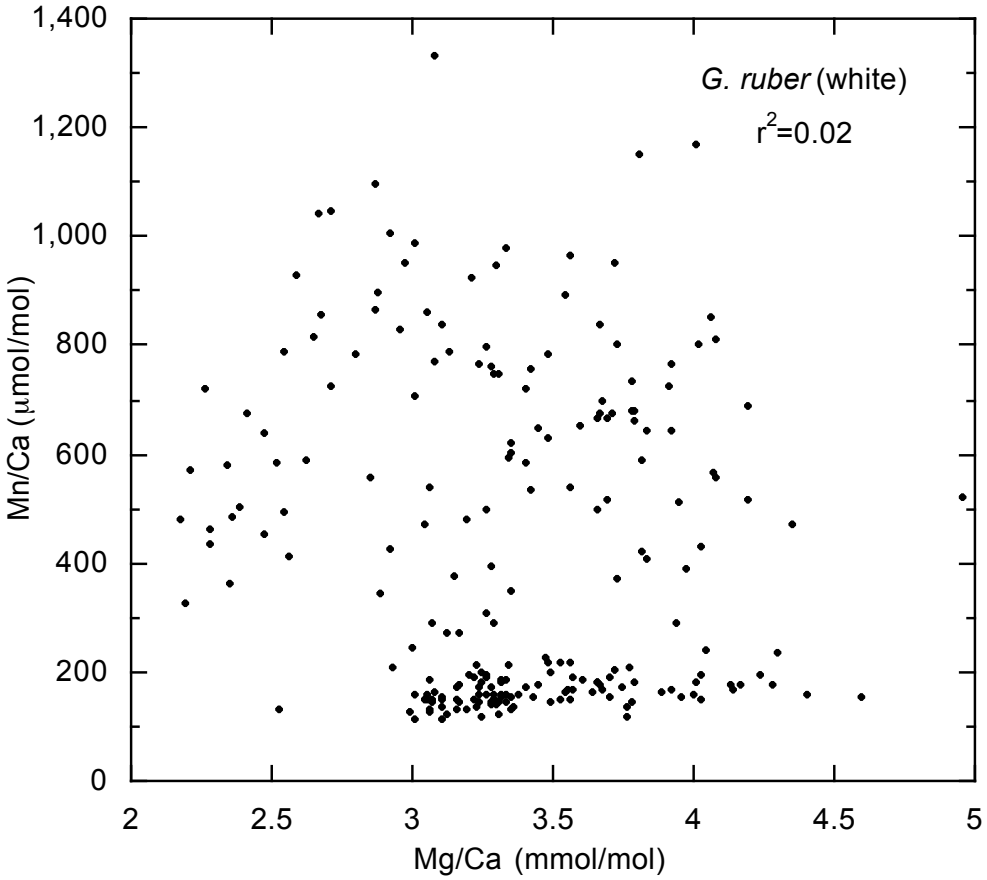

Figure S3. Comparison of culled *G. ruber* (white) Mg/Ca and Mn/Ca data. The lack of correlation between Mg and Mn suggests that Mg/Ca values are not influenced by Mn overgrowths.

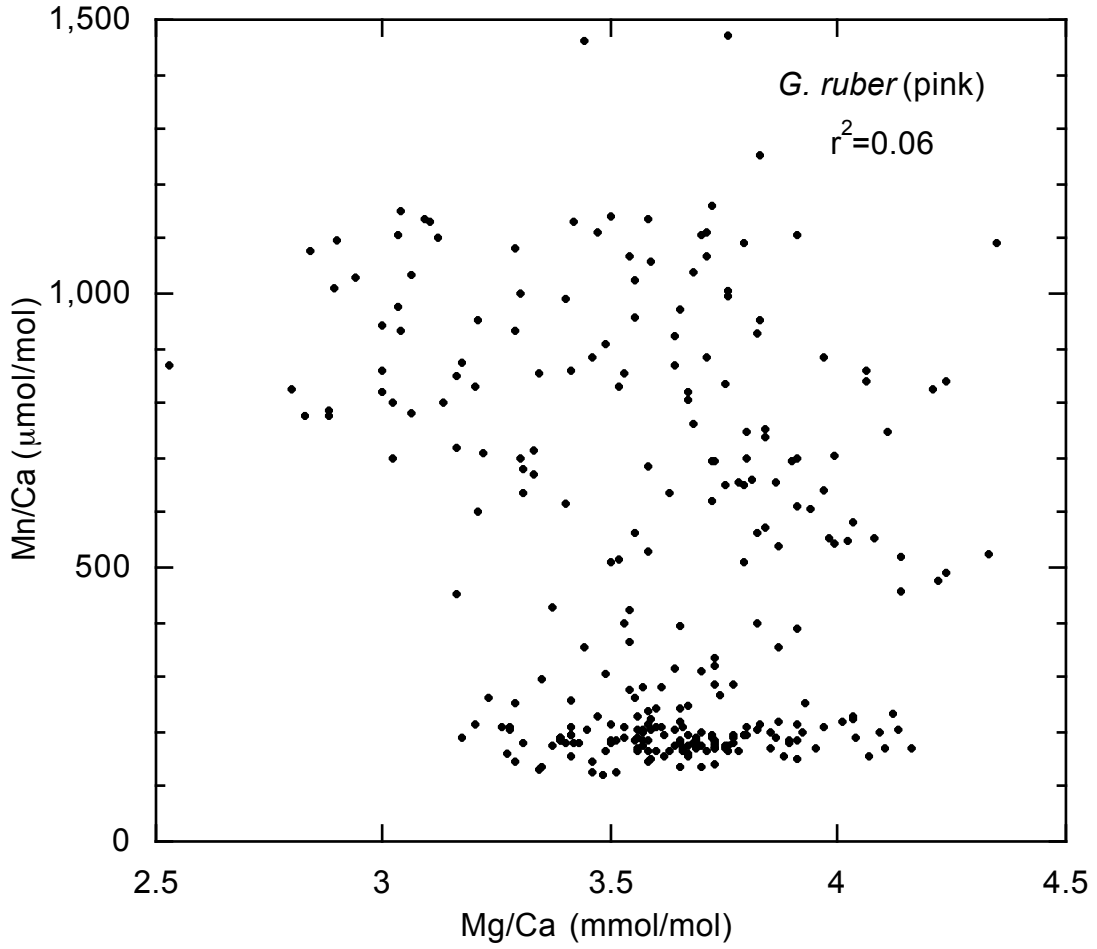

Figure S4. Comparison of culled *G. ruber* (pink) Mg/Ca and Mn/Ca data. The lack of correlation between Mg and Mn suggests that Mg/Ca values are not influenced by Mn overgrowths.

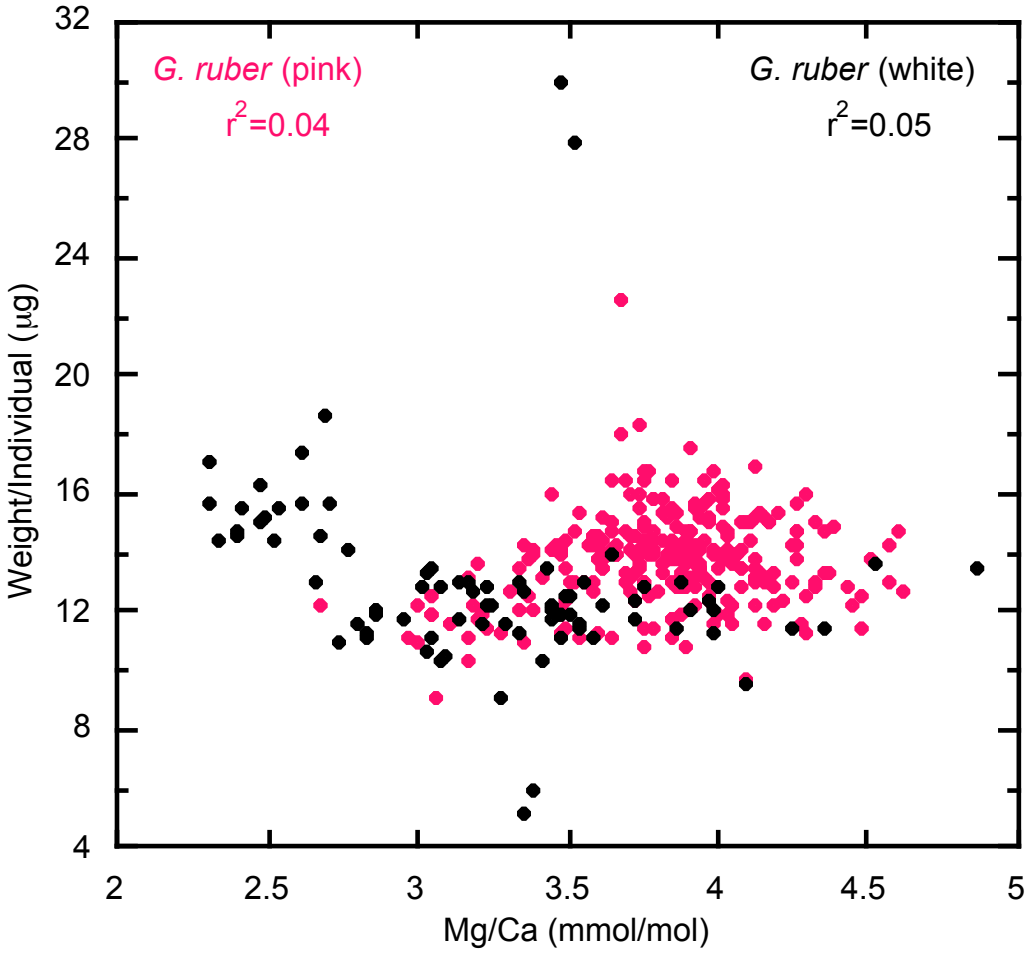

Figure S5. Comparison of all *G. ruber* (white and pink) Mg/Ca and weight per Foraminifera data. Both white and pink varieties show no correlation between Mg/Ca value and weight per individual.

Al and Fe have commonly been used to monitor the removal of Mg-rich clays adhered to foraminiferal tests. While no universal cutoff values are used for sufficient clay removal, most studies implement an Al or Fe threshold for rejecting Mg/Ca data points that are compromised by insufficient clay removal. While monitoring clay-contamination is important, the diversity of sediment compositions on which foraminiferal Mg/Ca-SST studies are based, suggests that no single threshold should be used globally.

Barker et al., (2003) typically observed Fe/Ca and Fe/Mg values at approximately 100 µmol/mol and 30 µmol/mol in foraminifera. Because Al was often undetectable on the inductively coupled plasma atomic emission spectrometer (ICP-AES) used in data generation, they rejected Mg/Ca measurements for samples with Fe/Mg values greater than 100 µmol/mol. In a different study, a Caribbean sediment core [Regenberg *et al.*, 2007] used Mg/Ca data with Fe/Ca values typically in the 200 µmol/mol range, which were double that of the values seen in the Barker et al. (2003) study. A Mg/Ca-SST record from the coast of South Africa did not use any threshold value and included all data points, including those over 200 µmol/mol [Martínez-

Méndez *et al.*, 2008]. Not only do these studies illustrate the variety of methods used to quantify the degree of clay contamination, but also the absence of universally accepted threshold value.

Additionally, regression analysis is a standard technique for investigating major clay contamination [Barker *et al.*, 2003; Schmidt *et al.*, 2004; Allison and Austin, 2008; Ferguson *et al.*, 2008; Yu *et al.*, 2008; Banakar *et al.*, 2010]. While the use of an Al or Fe threshold provides a more conservative Mg/Ca-SST record, the lack of correlation between Mg/Ca and Al/Ca (or Fe/Ca) values for the culled data set (once the threshold is applied) supports minimal to no effect of clay contamination on Mg/Ca-SST records. However, many studies simply state that the lack of correlation between Mg/Ca and Al/Ca (or Fe/Ca) and do not remove any Mg/Ca data points.

The Al/Ca threshold of 200 μmol/mol and the lack of correlation between Mg/Ca and Al/Ca used in our new Orca Basin *G. ruber* (white and pink) records are consistent with previous Mg/Ca-SST studies. Figures S6 and S7 indicate that when a lower Al/Ca threshold of 100 μmol/mol is applied to our data, the same climatic trends are visible.

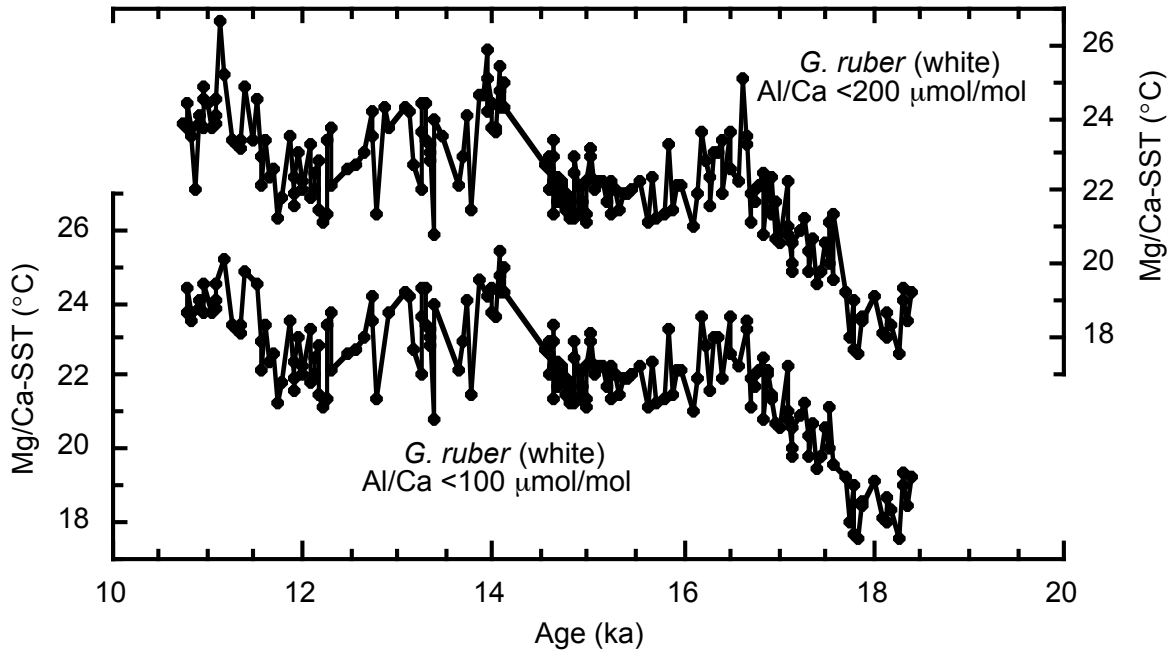

Figure S6. Comparison between *G. ruber* (white) with a <200 μmol/mol Al/Ca threshold (top panel) to *G. ruber* (white) with a <100 μmol/mol Al/Ca threshold. 21 more points were removed using the <100 μmol/mol threshold; however, the only obvious points are at 11.1 ka and 16.6 ka.

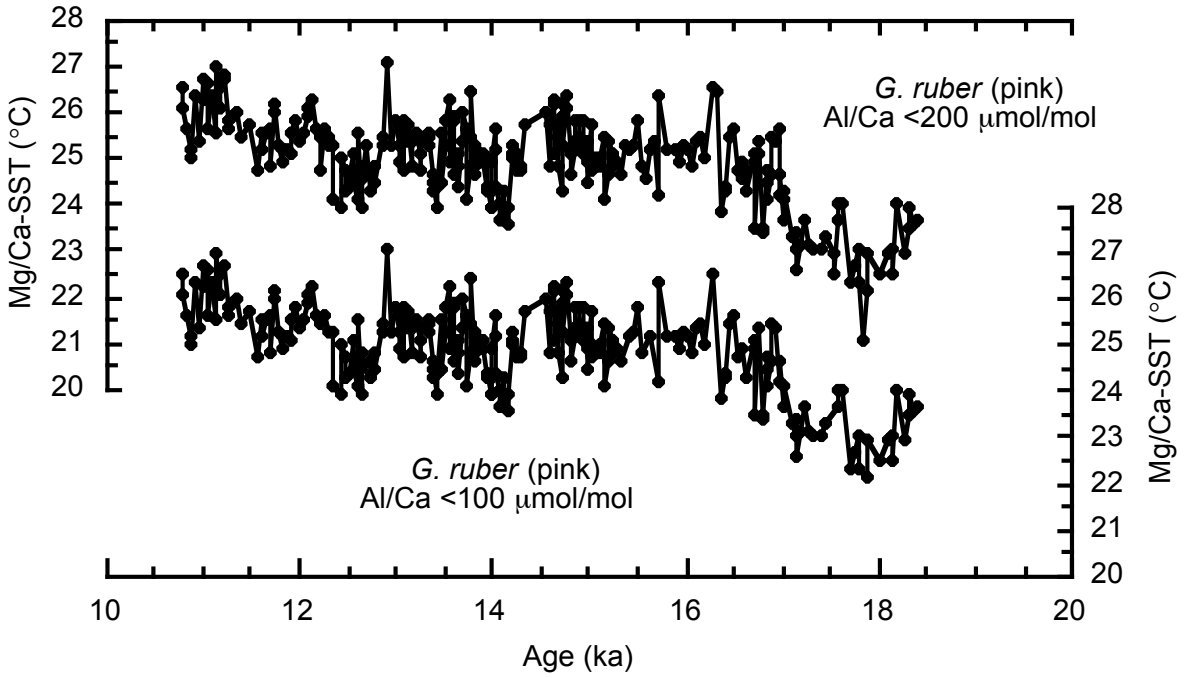

Figure S7. Comparison between *G. ruber* (pink) with a <200 μmol/mol Al/Ca threshold (top panel) to *G. ruber* (pink) with a <100 μmol/mol Al/Ca threshold. 19 more points were removed using the <100 μmol/mol threshold. In the *G. ruber* (pink) SST record, a visible high Mg/Ca-SST point (ex. 27°C at ~12.9 ka) has a very low Al/Ca value of ~16 μmol/mol. Furthermore, a low Mg/Ca-SST point is removed using the <100 μmol/mol Al/Ca threshold, which suggests that such a low Al/Ca threshold is removing Mg/Ca-SST data points not affected by Mg-rich clays.

2. Age Models and Radiocarbon Dates

Table S1. Radiocarbon age control for core MD02-2550.

Depth (cm)	CAMS ID	^{14}C age (ka)	± ^{14}C error (yrs)	Marine09 calibrated calendar age (ka)	+ calendar error (ka)	- calendar error (ka)
308	100676	9.790[a]	40	10.639	0.099	0.150
318	139344	9.965	35	10.946	0.195	0.154
329.5	130345	10.215	35	11.200	0.056	0.053
337.5	130346	10.500	45	11.658	0.274	0.246
342	137085	10.470	40	11.574	0.232	0.186
348	130347	10.660	45	12.001	0.178	0.186
357	130348	10.850	40	12.351	0.174	0.064
367	130349	10.925	40	12.456	0.120	0.140
*378		11.170	60	12.657	0.098	0.157
386.5	130350	11.375	40	12.828	0.167	0.149
389.5	137089	11.575	50	13.060	0.193	0.177
397.5	130351	11.855	40	13.317	0.118	0.109
407	130352	12.085	40	13.531	0.145	0.160
418.5	130354	12.515	40	13.953	0.144	0.157
427.5	130355	12.590	40	14.033	0.162	0.157
*435		12.910	60	14.662	0.461	0.410
441	130357	12.785	45	14.418	0.332	0.499
455	130359	12.800	40	14.437	0.328	0.491
466	130360	12.980	40	14.833	0.344	0.341
475	130362	12.805	40	14.444	0.329	0.490
485	137091	13.100	60	15.042	0.423	0.219
495	137092	13.145	50	15.111	0.246	0.450
505	137093	13.330	60	15.453	0.402	0.672
515	137094	13.610	80	16.106	0.724	0.557
525	137098	13.805	45	16.577	0.485	0.282
535	137099	13.860	50	16.640	0.324	0.241
545	137100	14.160	60	16.873	0.166	0.181
554	137101	14.160	70	16.873	0.176	0.193
564	137102	14.310	60	16.970	0.187	0.214
*565		14.470	60	17.105	0.238	0.355
574	137103	14.480	70	17.118	0.248	0.359
595	137104	14.870	100	17.599	0.408	0.323
604	137105	15.140	70	17.924	0.299	0.159
614	137106	15.460	80	18.248	0.233	0.318
650	142569	16.345	50	19.130	0.247	0.254

[a] All raw (no reservoir correction applied) ^{14}C dates are given in radiocarbon years before present.

*All dates were analyzed at Lawrence Livermore National Laboratory in Livermore, California, except those indicated by asterisk (*), which were analyzed at the Swiss Federal Institute of Technology, Zürich (ETH) and published in *Meckler et al.,* (2008). Calibration to calendar years is based on *Reimer et al.* (2009)

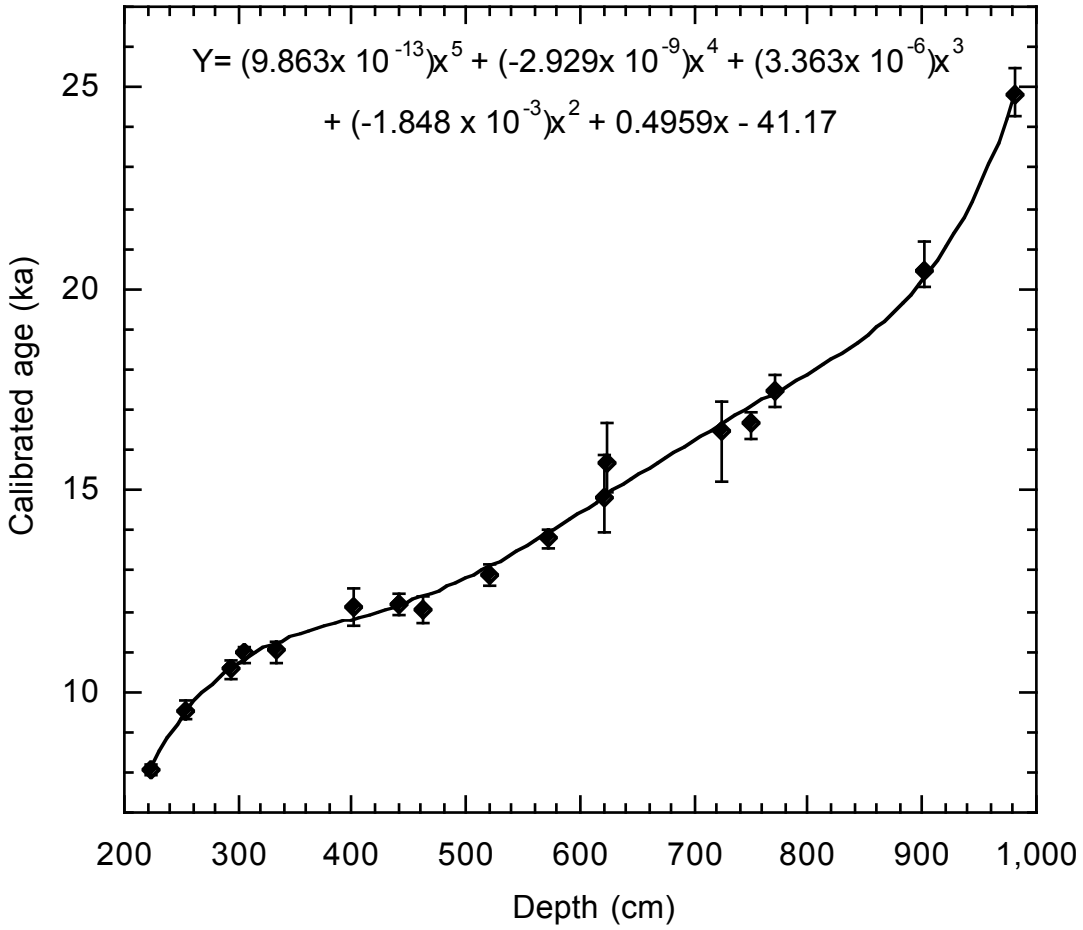

Figure S8. Revised Cariaco Basin [Lea *et al.*, 2003] age model based on the new Marine09 calibration [Reimer *et al.*, 2009]. Calendar years were calibrated using a 5th order polynomial.

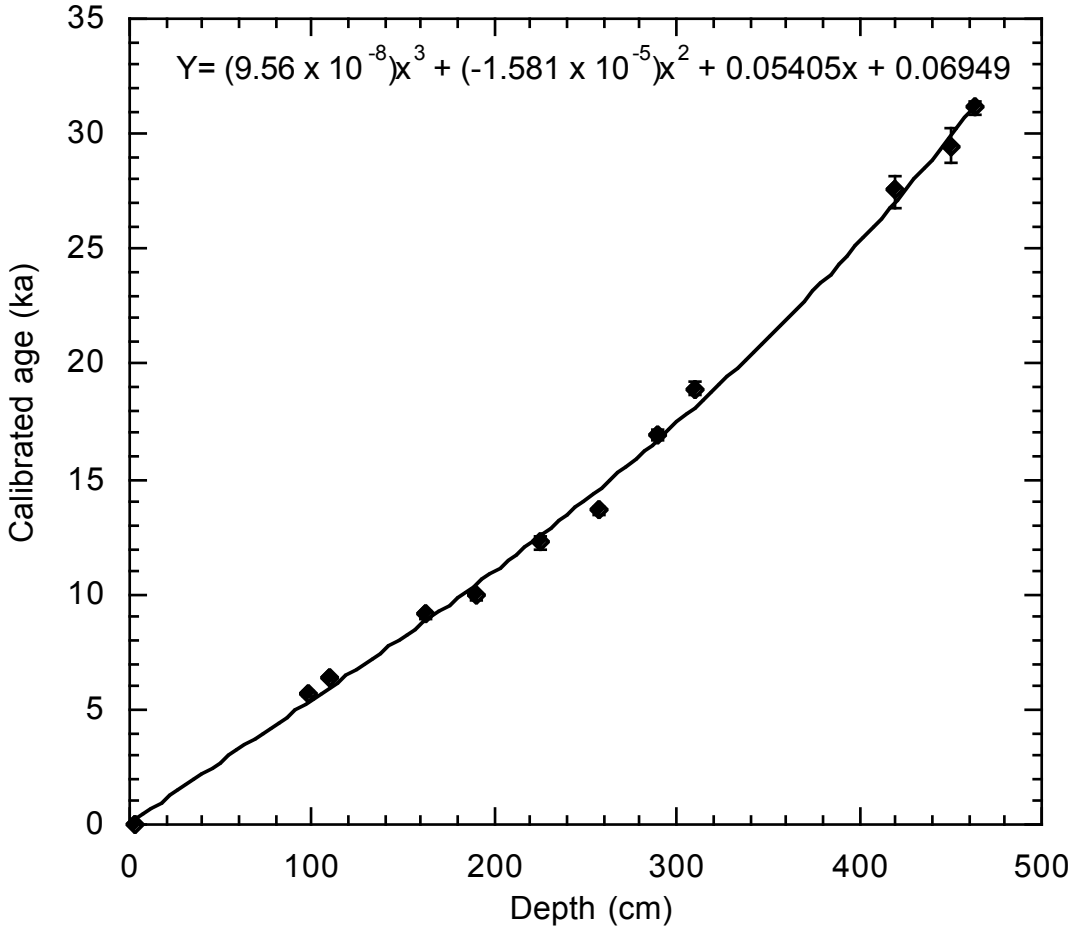

Figure S9. Revised Tobago Basin [Rühlemann *et al.*, 1999] age model based on the new on the new Marine09 calibration [Reimer *et al.*, 2009]. Calendar years were calibrated using a 3rd order polynomial.

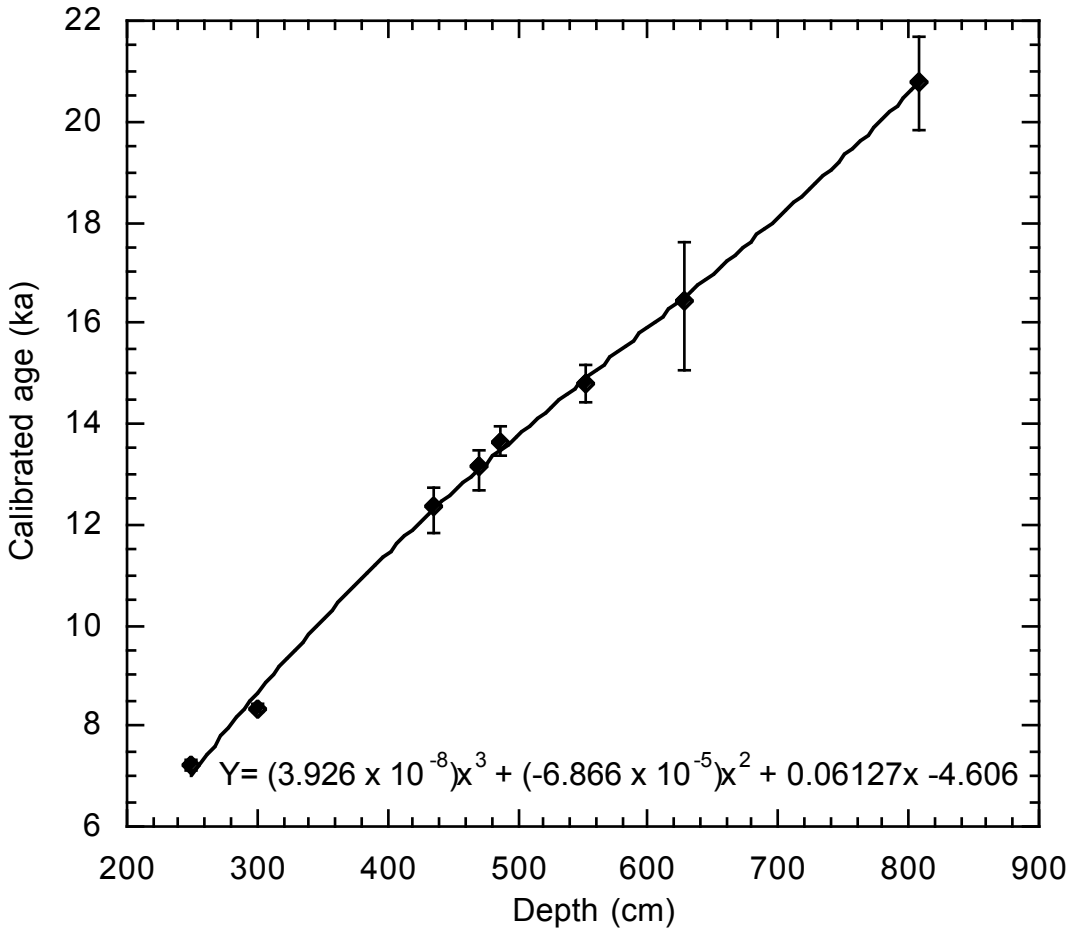

Figure S10. Revised GOM (core EN32-PC6) [Flower *et al.*, 2004] age model based on the new on the new Marine09 calibration [Reimer *et al.*, 2009]. Calendar years were calibrated using 3rd order polynomial.

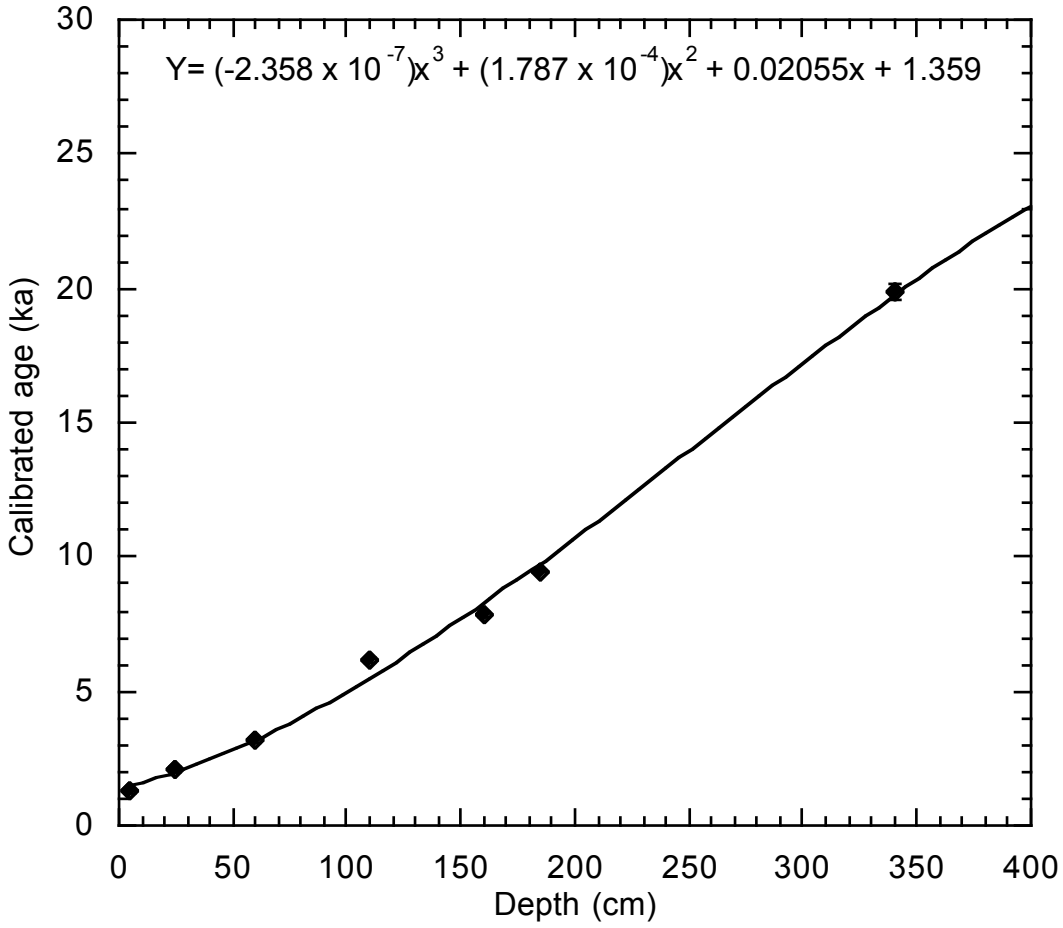

Figure S11. Revised GOM [Nürnberg *et al.*, 2008; Ziegler *et al.*, 2008] (core MD02-2575) age model based on the new on the new Marine09 calibration [Reimer *et al.*, 2009]. Calendar years were calibrated using a 3rd order polynomial.

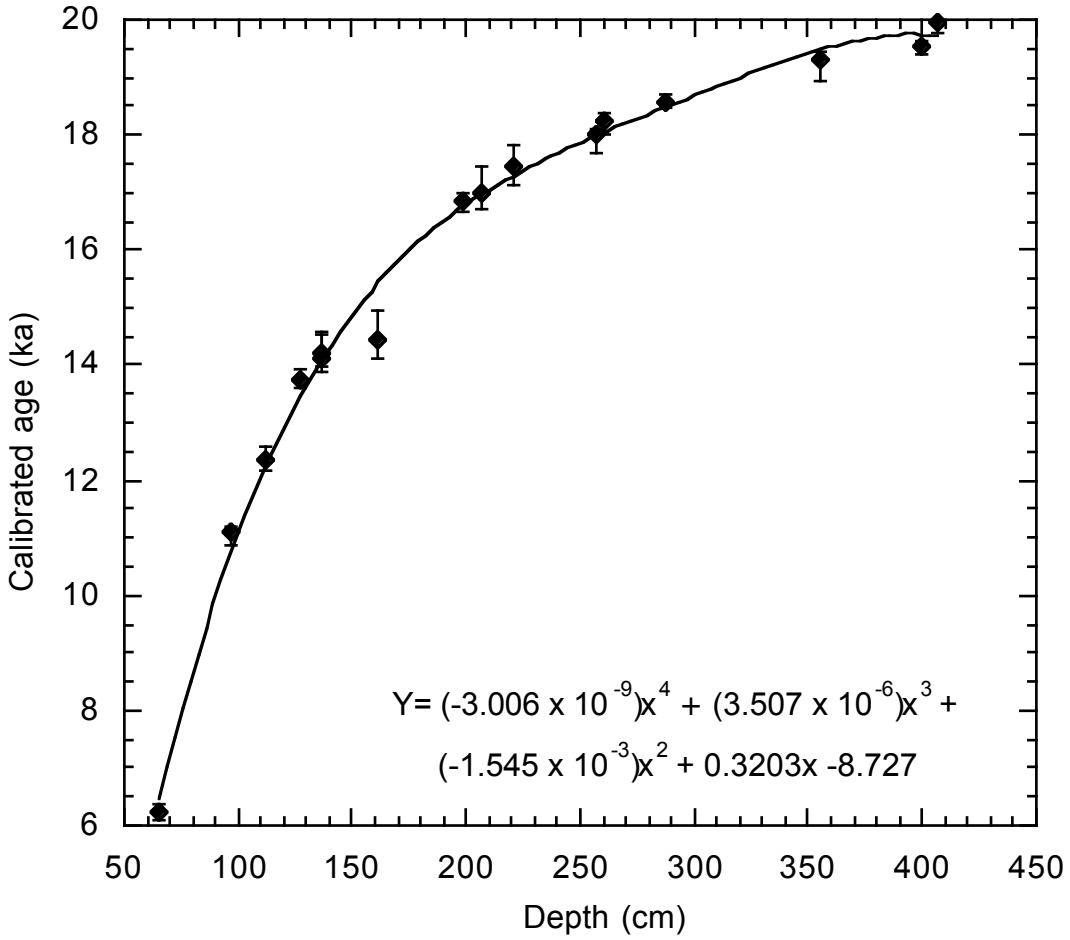

Figure S12. Revised 231Pa/230Th [McManus *et al.*, 2004] age model based on the new on the new Marine09 calibration [Reimer *et al.*, 2009]. Calendar years were calibrated using a 4th order polynomial.

Table S2. Revised radiocarbon dates for Cariaco Basin [Lea *et al.*, 2003].

Depth	^{14}C age (ka)	± ^{14}C error (yrs)	Marine09 calibrated calendar age (ka)	+ Calendar error (ka)	- Calendar error (ka)
223	7.58[a]	70	8.044	0.151	0.141
253	8.85	90	9.518	0.245	0.212
293	9.7	80	10.562	0.236	0.215
305	9.99	60	10.963	0.176	0.236
334	10.07	100	11.037	0.192	0.327
401	10.73	120	12.121	0.451	0.456
441	10.76	80	12.184	0.225	0.278
462	10.69	80	12.057	0.303	0.336
521	11.43	150	12.907	0.281	0.284
573	12.38	100	13.810	0.220	0.223
621	13.02	220	14.801	1.103	0.833
623	13.39	200	15.698	0.947	0.779
632	14.53[b]	310	17.270	0.733	0.622
641	14.41[b]	260	17.134	0.692	0.490
723	13.96	300	16.499	0.694	1.287
750	13.93	100	16.690	0.264	0.447
770	14.78	140	17.481	0.415	0.418
902	17.6	150	20.451	0.719	0.393
982	21.21	210	24.796	0.669	0.501

[a] All raw (no reservoir correction applied) ^{14}C dates are given in radiocarbon years before present. Calibration to calendar years is based on *Reimer et al.* (2009).
[b]Denotes ^{14}C dates that were not used in age model.

Table S3. Revised radiocarbon dates for Tobago Basin [Rühlemann *et al.*, 1999].

Depth	^{14}C age (ka)	± ^{14}C error (yrs)	Marine09 calibrated calendar age (ka)	+ Calendar error (ka)	- Calendar error (ka)
3	0.38 [a]	30	0		
98	5.30	50	5.660	0.140	0.095
110	5.92	40	6.335	0.093	0.077
163	8.48	60	9.106	0.172	0.138
190	9.15	50	9.942	0.186	0.208
225	10.80	90	12.248	0.308	0.296
257.5	12.22	70	13.662	0.162	0.212
290	14.21	90	16.908	0.231	0.192
310	16.14	100	18.881	0.406	0.222
420	23.23	210	27.554	0.557	0.730
450	25.06	260	29.499	0.727	0.756
463	27.03	-220 and +210	31.144	0.254	0.280

[a] All raw (no reservoir correction applied) ^{14}C dates are given in radiocarbon years before present. Calibration to calendar years is based on *Reimer et al.* (2009).

Table S4. Revised radiocarbon dates for Orca Basin core EN32-PC6 [Flower *et al.*, 2004].

Depth (cm)	^{14}C age (ka)	± ^{14}C error (yrs)	Marine09 calibrated calendar age (ka)	+ Calendar error (ka)	- Calendar error (ka)
250-252	6.680[a]	40	7.213	0.095	0.082
300-302	7.890	40	8.357	0.090	0.092
436-437	10.910	160	12.352	0.356	0.498
470-472	11.690	210	13.139	0.346	0.466
486-487	12.240	150	13.653	0.315	0.300
552-554	12.970	40	14.792	0.373	0.348
627-629	13.970	410	16.424	1.158	1.344
808-810	17.860	370	20.804	0.873	0.975

[a] All raw (no reservoir correction applied) ^{14}C dates are given in radiocarbon years before present. Calibration to calendar years is based on *Reimer et al.* (2009).

Table S5. Revised radiocarbon dates for DeSoto Canyon core MD02-2575 [Nürnberg *et al.*, 2008; Ziegler *et al.*, 2008].

Depth (cm)	^{14}C age (ka)	± ^{14}C error (yrs)	Marine09 calibrated calendar age (ka)	+ Calendar error (ka)	- Calendar error (ka)
5	1.700 [a]	25	1.260	0.047	0.077
25	2.430	30	2.068	0.092	0.104
60	3.310	30	3.165	0.109	0.120
110	5.755	30	6.187	0.081	0.095
160	7.370	40	7.839	0.091	0.107
185	8.810	40	9.477	0.059	0.072
340	17.150	80	19.904	0.297	0.336
585	23.050	140	27.319	0.531	0.526

[a] All raw (no reservoir correction applied) ^{14}C dates are given in radiocarbon years before present. Calibration to calendar years is based on *Reimer et al.* (2009).

Table S6. Revised radiocarbon for $^{231}Pa/^{230}Th$ data, the proxy for NADW production [McManus *et al.*, 2004].

Depth (cm)	^{14}C age (ka)	± ^{14}C error (yrs)	Marine09 calibrated calendar age (ka)	+ Calendar error (ka)	- Calendar error (ka)
65	5.82[a]	60	6.239	0.142	0.137
97	10.05	40	11.08	0.095	0.189
112	10.85	55	12.346	0.216	0.182
127	12.30	50	13.754	0.154	0.169
137	12.65	50	14.106	0.436	0.214
137	12.70	50	14.209	0.388	0.248
161	12.80	50	14.443	0.498	0.341
199	14.10	50	16.832	0.173	0.167
207	14.30	150	16.989	0.451	0.267
221	14.75	65	17.443	0.368	0.322
257	15.20	80	18.003	0.120	0.341
261	15.50	70	18.249	0.140	0.223
287	15.65	60	18.547	0.137	0.082
355	16.55	80	19.285	0.166	0.351
400	16.85	80	19.553	0.065	0.142
407	17.20	90	19.963	0.305	0.199

[a] All raw (no reservoir correction applied) ^{14}C dates are given in radiocarbon years before present. Calibration to calendar years is based on *Reimer et al.* (2009).

3. Orca Basin Sediments and Redox Conditions

Orca Basin is a unique environmental and depositional setting, where excellent preservation of organic and inorganic matter is attributed to a large, 220 m deep brine lake within the basin [*Sackett et al.*, 1977; *Pilcher and Blumstein*, 2007]. The brine lake itself, with an area of ~123 km^2, was formed from the exposure and dissolution of a salt diapir derived from the Jurassic Louann Evaporite Formation at about 8.0 ka [*Addy and Behrens*, 1980]. There is a transition in core MD02-2550 between 201-203 cm from laminated gray mud high in manganese oxides to laminated, sulfide- and organic-rich black mud which suggests a decrease in O_2 concentration to a highly saline anoxic environment [*Addy and Behrens*, 1980].

The degradation of organic matter in marine sediments follows a specific pathway of redox-reactions, based on the availability of oxygen and other electron acceptors [*Froelich et al.*, 1979]. The oxidation of organic matter using particulate manganese (IV) oxide produces

reduced manganese, typically as dissolved Mn(II) in sedimentary pore water. The dissolved Mn(II) diffuses up into the sediment to overlying oxygenated waters, where Mn(II) is re-oxidized and precipitated as manganese (IV) oxide.

Iron (III) oxides and iron (III) hydroxides may also serve as electron acceptors in low-oxygen conditions. In oxic sediments, where magnetite and other iron oxides dominate, high magnetic susceptibility is observed. However, when oxygen levels decrease and sediments become reducing and alternate electron acceptors such as iron oxides are used to degrade organic matter, the magnetite is reduced to Fe (II), which subsequently yields low magnetic susceptibility values [*Bloemendal et al.*, 1992]. In summary, oxic sediments should be dominated by magnetite and other iron oxides, which are high in magnetic susceptibility. In reducing sediments, magnetite and other iron oxides are reduced to Fe (II) and yield low magnetic susceptibility.

Core MD02-2550 exhibits multiple intervals of faintly to strongly laminated sediments (Figure S13). From approximately 18.4-17.3 ka, no laminations are present. At 17.3 ka, faint laminations appear and from 16.6-12.4 ka, strong laminations are present. Very faint laminations are seen from 12.4-10.7 ka. These laminations, due to the lack of bioturbation, likely during anoxic intervals, which suggests that anoxic conditions existed prior to brine lake formation.

Magnetic susceptibility and elemental analyses from core MD02-2550 provide new insights on the controls of sediment laminations and redox conditions in Orca Basin during the last deglaciation. Low field magnetic susceptibility was measured using a small diameter Bartington coil on board the R/V *Marion Dufresne* in 2002. Magnetic susceptibility values average 14.2 κ (10^{-6} SI) from 18.4-17.0 ka and 13.0-10.7 ka, but decrease to 7.2 κ (10^{-6} SI) from 16.6-13.0 ka (Figure S13), suggesting a transition to low-oxygen conditions. During the same

intervals, Mn/Ca data from *G. ruber* foraminiferal tests also exhibit a decrease in mean values from 675 to 173 μmol/mol suggesting that minimal Mn-Fe oxide coatings are present on *G. ruber* tests. Although these coatings may be enriched in Mg [*Boyle*, 1983], which may affect SST calculations, the lack of correlation between Mn/Ca and Mg/Ca indicates that these coatings are low in Mg (Figures S3 and S4). The large decrease in Mn/Ca values at 16.6-13.0 ka suggests that *G. ruber* are recording post-depositional geochemical sedimentary conditions in Orca Basin. Specifically, *G. ruber* Mn/Ca ratios and magnetic susceptibility data suggest anoxic conditions from 16.6-13.0 ka.

Anoxic conditions in Orca Basin may have been enhanced by an increase in nutrient and terrestrial organic material input from the North American continent due to Laurentide Ice Sheet (LIS) meltwater. Elevated nutrient concentrations allow for enhanced productivity, which deplete bottom water oxygen levels during respiration, eliminate bioturbation, and allow laminations to form. Previous research from Orca Basin indicates an increased delivery of reworked terrestrial organic matter [*Meckler et al.*, 2008] from ~17.0-14.0 ka which coincides with stronger laminations and decreased magnetic susceptibility and Mn/Ca ratios and supports low oxygen conditions.

Magnetic susceptibility and elemental analyses provide insight into the controls of sediment laminations and redox conditions in Orca Basin. Both magnetic susceptibility and Mn/Ca ratios of *G. ruber* suggest very low oxygen conditions within Orca Basin at 16.4-13.1 ka. The presence of laminations from 16.4-12.4 ka suggests a linkage between low oxygen levels, redox conditions and lack of bioturbation. Additionally, laminations and anoxia may be driven by an increase in terrestrial organic input to the basin and enhanced primary productivity. This

study highlights that elemental geochemistry in Foraminifera can be used to elucidate post-depositional sediment conditions.

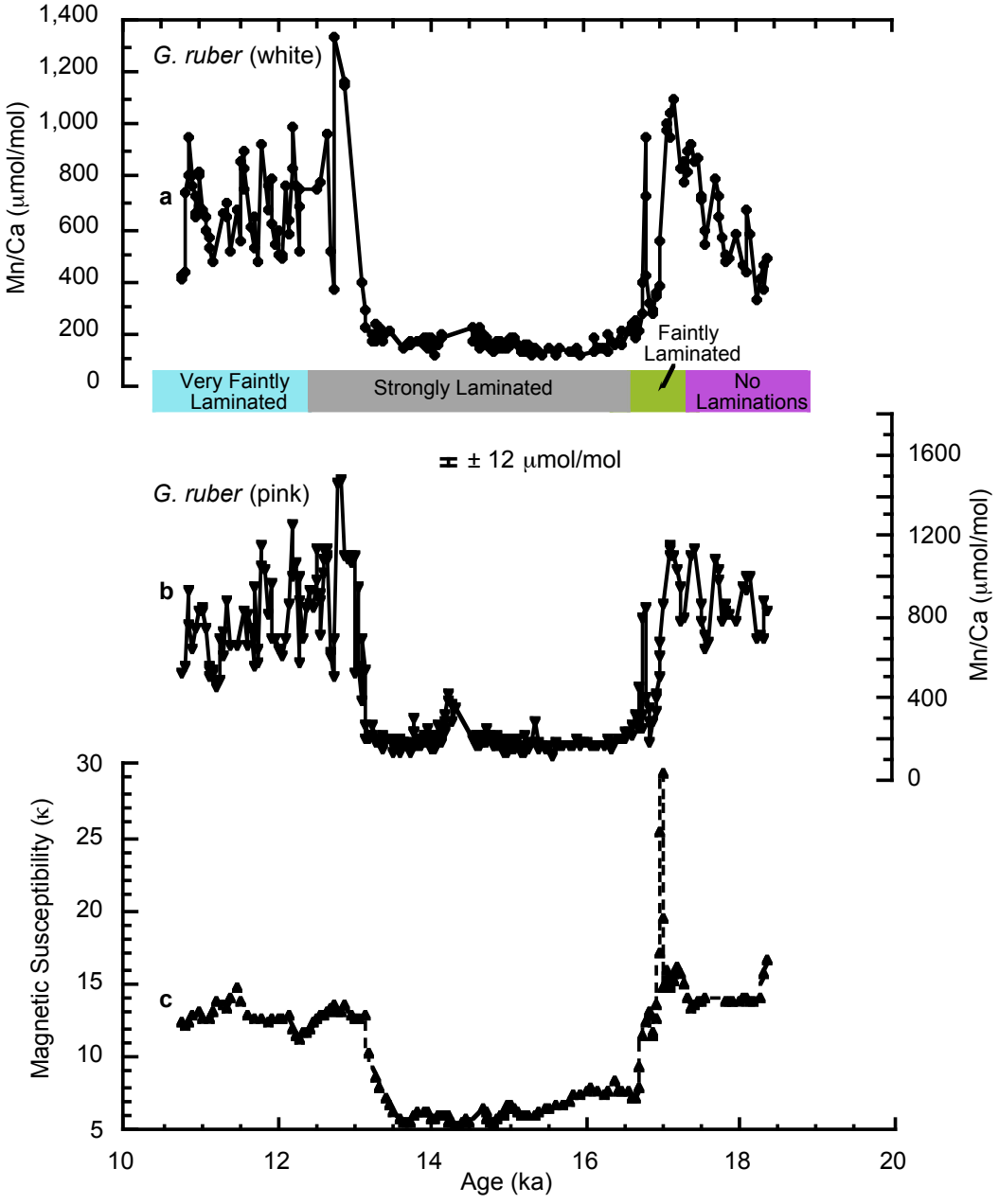

Figure S13. Comparison of Mn/Ca ratios of (**a**) *G. ruber* (white), (**b**) *G. ruber* (pink) and (**c**) magnetic susceptibility from core MD02-2550. Both records show decreased values from 16.6-13.0 ka. Correlation between Mn/Ca data, magnetic susceptibility and sediment laminations is consistent with a redox influence on *G. ruber* Mn/Ca data.

References

Addy S. K., Behrens E. W. (1980), Time of accumulation of hypersaline anoxic brine in Orca Basin (Gulf of Mexico), *Marine Geology, 37,* 241-252 10.1016/0025-3227(80)90104-8.

Allison N., Austin W. E. N. (2008), Serial Mg/Ca and Sr/Ca chronologies across single benthic foraminifera tests, *Chem. Geol., 253,* 83-88 10.1016/j.chemgeo.2008.04.010.

Banakar V. K., Mahesh B. S., Burr G. S., Chodankar A. R. (2010), Climatology of the Eastern Ababian Sea during the last glacial cycle reconstructed from paired measurment of foraminiferal $\delta^{18}O$ and Mg/Ca, *Quaternary Research, 73,* 535-540 10.1016/j.yqres.2010.02.002.

Barker S., Greaves M., Elderfield H. (2003), A study of cleaning procedures used for foraminiferal Mg/Ca paleothermometry, *Geochemistry, Geophysics, Geosystems, 4,* 1-20 10.1029/2003GC000559.

Bloemendal J., King J. W., Hall F. R., Doh S.-J. (1992), Rock Magnetism of Late Neogene and Pleistocene Deep-Sea Sediments: Relationship to Sediment Source, Diagenetic Processes, and Sediment Lithology, *J. Geophys. Res., 97,* 4361-4375

Boyle E. (1983), Manganese carbonate overgrowths on foraminifera tests, *Geochim. Cosmochim. Acta, 47,* 1815-1819

Ferguson J. E., Henderson G. M., Kucera M., Rickaby R. E. M. (2008), Systematic change of foraminiferal Mg/Ca ratios across a strong salinity gradient, *Earth Planet. Sci. Lett., 265,* 153-166 10.1016/j.epsl.2007.10.011.

Flower B. P., Hastings D. W., Hill H. W., Quinn T. M. (2004), Phasing of deglacial warming and Laurentide Ice Sheet meltwater in the Gulf of Mexico, *Geology, 32,* 597-600 10.1130/G20604.1.

Froelich P. N., Klinkhammer G. P., Bender M. L., Luedtke N. A., Heath G. R., Cullen D., Dauphin P., Hammond D., Hartman B. (1979), Early Oxidation of organic matter in pelagic sediments of the eastern equatorial Atlantic: suboxic diagenesis, *Geochim. Cosmochim. Acta, 43,* 1075-1090

Lea D. W., Pak D. K., Peterson L. C., Hughen K. A. (2003), Synchroneity of Tropical and High-Latitude Atlantic Temperatures over the Last Glacial Termination, *Science, 301,* 1361-1364

Martínez-Méndez, Zhan R., Hall I. R., Pena L. D., Cacho I. (2008), 345,000-year-long multi-proxy records off South Africa document variable contributions of Northern versus Southern Component Water to the Deep South Atlantic, *Earth Planet. Sci. Lett., 267,* 309-321 10.1016/j.epsl.2007.11.050.

McManus J. F., Francois R., Gherardi J. M., Keigwin L. D., Brown-Leger S. (2004), Collapse and rapid resumption of Atlantic meridional circulation linked to deglacial climate changes, *Nature, 428,* 834-837

Meckler A. N., Schubert C. J., Hochuli P. A., B.Plessen, Birgel D., Flower B. P., Hinrichs K.-U., Haug G. H. (2008), Glacial to Holocene terrigenous organic matter input to sediments from Orca Basin, Gulf of Mexico-A combined optical and biomarker approach, *Earth Planet. Sci. Lett., 272,* 251-263

Nürnberg D., Ziegler M., Karas C., Tiedemann R., Schmidt M. W. (2008), Interacting Loop Current variability and Mississippi River discharge over the past 400 kyr, *Earth Planet. Sci. Lett., 272,* 278-289

Pilcher R. S., Blumstein R. D. (2007), Brine volume and salt dissolution rates in Orca Basin, northeast Gulf of Mexico, *AAPG Bulletin, 91,* 823-233

Regenberg M., Nürnberg D., Schönfeld J., Reichart G.-J. (2007), Early diagenetic overprint in Caribbean sediment cores and its effect on the geochemical composition of planktonic foraminifera, *Biogeosciences, 4,* 957-973

Reimer P. J., Baillie M. G. L., Bard E., Bayliss A., Beck J. W., Blackwell P. G., Ramsey C. B., Buck C. E., Burr G. S., Edwards R. L., Friedrich M., Grootes P. M., Guilderson T. P., Hajdas I., Heaton T. J., Hogg A. G., Hughen K. A., Kaiser K. F., Kromer B., McCormac F. G., Manning S. W., Reimer R. W., Richards D. A., Southon J. R., Talamo S., Turney C. S. M., van der Plicht J., Weyhenmeyer C. E. (2009), Incal09 and Marine09 radiocarbon age calibration curves, 0-50,000 years cal B.P, *Radiocarbon, 51,* 1111-1150

Rühlemann C., Mulitza S., Müller P. J., Wefer G., Zahn R. (1999), Warming of the tropical Atlantic Ocean and slowdown of thermohaline circulation during the last deglaciation, *Nature, 402,* 511-514

Sackett W. M., Bernard B. B., Brooks J. M. (1977), Chemical measurements in Orca Basin sediments:, *Eos, Transactions of the America Geophysical Union, 58,* 1175-

Schmidt M. W., Spero H. J., Lea D. W. (2004), Links between salinity variation in the Caribbean and North Atlantic thermohaline circulation, *Nature, 428,* 160-163

Yu J., Elderfield H., Jin Z., Booth L. (2008), A strong temperature effect on U/Ca in planktonic foraminifera carbonates, *Geochim. Cosmochim. Acta, 72,* 4988-5000

Ziegler M., Nürnberg D., Karas C., Tiedemann R., Lourens L. J. (2008), Persistent summer expansion of the Atlantic Warm Pool during glacial abrupt cold events, *Nature Geo., 1,* 601-605